Set Down Study of Projectile in Flight Through Imaging

Suman Kumar Choudhury[*], Pankaj Kumar Sa, Banshidhar Majhi, and Tapan Kumar Biswal[#]

[#]*Proof and Experimental Establishment, DRDO, Chandipur-756 025, India*
[*]*National Institute of Technology, Rourkela-769 008, India*
[*]*E-mail: suman.winter@gmail.com*

ABSTRACT

Deformation study of projectile immediately after firing is essential for its successful impact. A projectile that undergoes more than the tolerated amount of deformation in the barrel may not produce the requisite results. The study of projectile deformation before its impact requires it to be imaged in flight and perform some computation on the acquired image. Often the deformation tolerance is of the order of tens of micrometer and the acquired image cannot produce image with such accuracy because of photographic limitations. Therefore, it demands sub-pixel manipulation of the captured projectile image. In this work the diameter of a projectile is estimated from its image which became blur because of slow shutter speed. First the blurred image is restored and then various interpolation methods are used for sub-pixel measurement. Two adaptive geometrical texture based interpolation schemes are also proposed in this research. The proposed methods produce very good results as compared to the existing methods.

Keywords: Deblurring, sub-pixel, image interpolation, scaling, geometrical texture, edge orientation, Newton polynomial

1. INTRODUCTION

Study of projectile behaviours closer to launcher is often desirable. An accurate measurement of projectile deformation immediately after firing is necessary for the successful impact. Deformation above the tolerance may not be effectual in producing intended result. Traditionally, diameters at different points of the cylindrical portion of the projectile are measured precisely before firing. After firing, the projectiles are collected and again measurements are taken at the same points. The differences give the deformation.

In this paper, the authors have investigated the above behaviour through in-flight image processing[1]. The deformation measurement is of the order of micrometer. For such an investigation, the projectile image is required to be captured soon after it is released from the muzzle. There is every possibility that the image obtained would be blurred because of the speed of the projectile. Use of very high speed camera can freeze the motion, and thereby a blur-free image can be acquired. However the state-of-the-art camera available nowadays cannot detect the micrometer deformation in the projectile because of its sensor limitations. The micrometer deformation demands sub-pixel manipulation of the projectile image. Existing interpolation methods[2] can be employed to compute missing pixel values. In addition, the authors have proposed two adaptive, edge oriented interpolation schemes.

The first proposed method selects the 4×4 neighbourhood of the missing pixel and constructs 19 adaptive windows based on regular geometrical texture shape. The next task is to find the smoothest window, which is computed based on variance of intensity values within each window. The smoothest block represents the edge direction, which is used for interpolating missing pixel. An exponential weight measure is chosen so that pixels closer to the re-sampling pixel are given more weight and vice versa.

In the second method, the authors have used Newton polynomial for interpolating missing pixel values. The second- and fourth-order difference of contiguous pixels gray values are computed to determine the edge orientation. Consequently, an adaptive function is inferred based on the texture alignment and the polynomial.

2. PROBLEM STATEMENT

The goal is to estimate the deformation with respect to diameter of a projectile in the order of micrometer through in-flight imaging. Considering the exposure time and projectile velocity into account, it has been deduced that the acquired images will become blur out of motion. Further, the projectile image demands sub-pixel manipulation. The mathematical formulation of the problem statement is given below:

- Shell diameter = 40 mm
- Camera resolution = 320 × 736
- Focal length = 300 mm
- Single-pixel resolution in object plane = 0.3123 mm
- Required measurable set down = 0.01 mm
- Sub-pixel accuracy factor = 0.3123/0.01 = 31.23 ≈ 32

The following objectives are identified to counter the above problems in estimating the deformation.

- Identification of notch-free part of projectile in the input

image.
- Computation of blur length and point spread function (PSF) estimation.
- Deblurring of the input image with the estimated PSF.
- Sub-pixel interpolation of deblurred image
- Detection of projectile contour (edge)
- Computation of diameter.

3. RELATED WORK

Pixel level edge-detection limits the dense knowledge about the real world object. Each pixel is linked to one sensor of the camera. High resolution camera can access more detailed information in the expense of higher cost. Various image processing mechanisms and statistical knowledge are comprised to access the sub-pixel information. Usually moment based methods[3] and interpolation mechanisms are employed for this purpose.

Non-adaptive interpolation methods include traditional algorithms like nearest neighbour, bilinear, bicubic, sinc interpolation, etc. Unlike traditional methods, adaptive algorithms[4-5] includes the gradient direction and edge orientation[6-7] information. The efficacy of any interpolation scheme is influenced by two elements[8]: visual quality of the scaled image and its time complexity. Most of the reported non-adaptive schemes suffer from undesirable artifacts such as blurring, aliasing, edge halos, especially in texture region of the image[9]. Adaptive interpolation mechanisms are applied to produce superior results. However, these advanced algorithms have high computational overload[10].

4. PROPOSED METHODOLOGIES

In this section, we detailed all the necessary steps required for the computation of projectile diameter. The block diagram for the overall procedure is shown in Fig. 1.

4.1 Input Image Normalisation

The ROI portion here refers to the cylindrical part of the projectile. Accordingly, the authors do necessary crop operation. The input image is normalised in the range 0 to 1, which is obtained by dividing each pixel value by the maximum intensity value of the image. Let O be the original image. The normalised image g is given by:

$$g = \frac{O}{\max(O)} \tag{1}$$

4.2 Blur Length Computation, PSF Estimation, and Motion Deblurring

The in-flight image gets blurred due to motion of the projectile. The motion length ML is computed as,

$$ML = \frac{v \times t}{l} \tag{2}$$

Here v, t and l denote the velocity of the projectile (m/s), exposure time of the camera (s), and single-pixel length in object plane, respectively. The two-dimensional point spread function (PSF) is estimated using the procedure[1].

One can use either the well-known iterative Lucy-Richardson algorithm[11] or Improved Iterative Blind Image
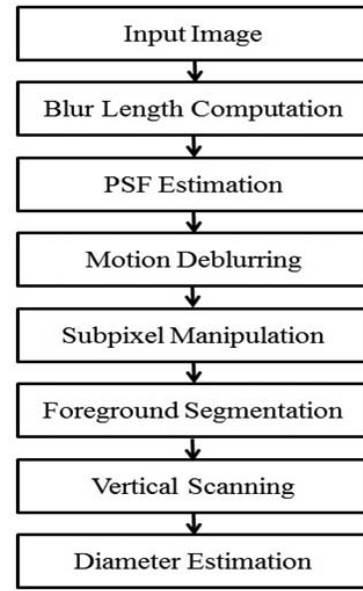
Figure 1. Block diagram of the overall procedure.

Deconvolution (IIBID) algorithm[12] for deblurring the cropped normalised image.

4.3 Sub-Pixel Manipulation

We have employed interpolation mechanism to compute sub-pixel measurement. Existing methods like Nearest Neighbor, Bilinear, Bicubic, and Lanczos re-sampling are used for this purpose. In addition, we have proposed two adaptive, edge-oriented interpolation schemes, as given below.

4.3.1 Method 1

The re-sampling pixel value is influenced by the local smoothness of pixels in neighbourhood, especially in the high frequency regions of the image. Our proposed scheme divides the neighbourhood kernel into different regions based on the shifting of high frequencies in different directions. For each missing pixel location, first its 4×4 neighbourhood window is considered. The next task is to divide this window to 19 different adaptive regions, as shown in Fig. 2, where each region indicates a geometrical regularity (possible edge orientation). The next task is to compute variance of intensity values for all 19 blocks. Block having minimum variance is chosen for re-sampling, because the smoothest block represents along-edge direction. To compute weight to the sampling point (x_p, y_p) inside the smoothest window, an exponential distance measure is chosen corresponding to the re-sampling point (x, y) as:

$$W(p) = e^{-\frac{1}{2}\left(dx^2 + dy^2\right)} \tag{3}$$

where dx^2 and dy^2 are the Euclidian distance between sampling location (x_p, y_p) from the re-sampling location (x, y). To compute the re-sampling point $f(x, y)$, the weighted mean of the interpolation kernel is computed as:

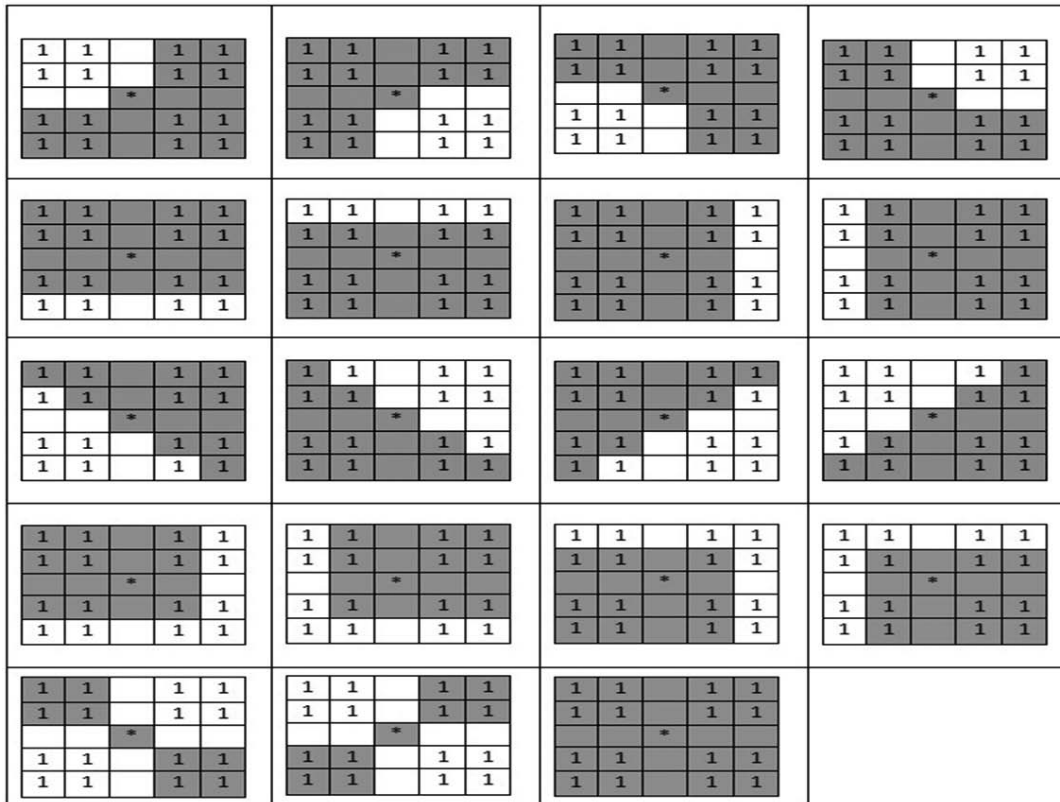$$f(x, y) = \frac{\sum_{i=1}^{k} (W_i \times f_i)}{\sum_{i=1}^{k} W_i} \tag{4}$$

Figure 2. Adaptive window formed by possible edge orientation based on geometrical regularities. ∗ represents the re-sampling pixel and gray-shaded region imply possible edge orientation.

Here k represents the smoothest window size and value of k is less than or equal to 16, which depends on local degree of smoothness and f_i, W_i represents the pixel value and weight at i^{th} location in the smoothest window respectively.

4.3.2 Method 2

In this approach, both second- and fourth-order Newton polynomial were used to assign missing pixel values. The third-order polynomial is asymmetric; as a result it cannot be used for interpolation. Two-dimensional image interpolation operates in two perpendicular directions; horizontal re-sampling followed by vertical re-sampling or vice-versa. The second and fourth-order Newton polynomial selects 3 and 5 adjacent pixels in one direction, respectively.

Given the equally spaced space function, $f(x)$ is expressed as $f(x_i) = f_i$, $i = 0, 1, 2, \ldots$ the second- and fourth-order polynomial can be represented by

$$P_2(x) = f_0 + \Delta f_0 t + \Delta^2 f_0 \frac{t(t-1)}{2} \qquad (5)$$

$$P_4(x) = f_0 + \Delta f_0 t + \Delta^2 f_0 \frac{t(t-1)}{2} + \Delta^3 f_0 \frac{t(t-1)(t-2)}{6} + \\ \Delta^4 f_0 \frac{t(t-1)(t-2)(t-3)}{24} \qquad (6)$$

Our proposed scheme first decides the texture alignment and accordingly selects neighbourhood pixels for interpolation. Each re-sampling pixel selects the closest 6×6 neighbourhood of known pixels. The relationship between the unknown and adjacent known pixels in one direction is shown in Fig. 3.

The absolute value of second- and fourth-order difference among adjacent pixels is computed to determine the edge orientation. In Fig. 3, the edge direction is decided by the smallest among the four measures,

$$\left|\Delta^2 f_0\right| = |f_2 - 2f_1 + f_0|$$

$$\Delta^2 f_1 = |f_3 - 2f_2 + f_1|$$

$$\left|\Delta^4 f_0\right| = |f_4 - 4f_3 + 6f_2 - 4f_1 + f_0|$$

$$\left|\Delta^4 f_1\right| = |f_5 - 4f_4 + 6f_3 - 4f_2 + f_1|$$

$$\Delta f_{\min} = \min\left\{\Delta^2 f_0\left|, \right|\Delta^2 f_1\left|, \right|\Delta^4 f_0\left|, \right|\Delta^4 f_1\right|\right\}$$

Thus, adaptive function to calculate the intensity of the re-sampling pixel (∗) is given by,

4.4 Foreground Segmentation

This process converts the cropped interpolated gray scale image to a binary image. The authors have used the optimal global thresholding Otsu method[1] for binarisation. Pixels having intensity value 0 and 1 represent the background and foreground regions, respectively.
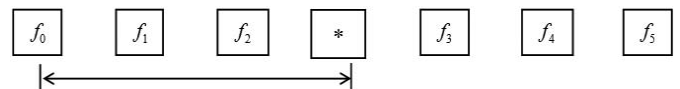

Figure 3. Relationship between re-sampling pixel and adjacent neighbourhood pixels.

$$f(*)= \begin{cases} f_0 + \Delta f_0 t + \Delta^2 f_0 \dfrac{t(t-1)}{2}, & if \ \Delta f_{min} = |\Delta^2 f_0| \\[2ex] f_1 + \Delta f_1 t + \Delta^2 f_1 \dfrac{t(t-1)}{2}, & if \ \Delta f_{min} = |\Delta^2 f_1| \\[2ex] f_0 + \Delta f_0 t + \Delta^2 f_0 \dfrac{t(t-1)}{2} + \Delta^3 f_0 \dfrac{t(t-1)(t-2)}{6} + \Delta^4 f_0 \dfrac{t(t-1)(t-2)(t-3)}{24}, & if \ \Delta f_{min} = |\Delta^4 f_0| \\[2ex] f_1 + \Delta f_1 t + \Delta^2 f_1 \dfrac{t(t-1)}{2} + \Delta^3 f_1 \dfrac{t(t-1)(t-2)}{6} + \Delta^4 f_1 \dfrac{t(t-1)(t-2)(t-3)}{24}, & if \ \Delta f_{min} = |\Delta^4 f_1| \end{cases} \quad (7)$$

4.5 Vertical Scanning

Here, each vertical line of the binary image is scanned two times: mid-point-to-bottom and mid-point-to-top (Here mid-point is the median point of each vertical line) until the first foreground edge point in each case is found and the difference of the two edge points is stored in an array named boundary.

4.6 Diameter Estimation

The boundary array contains the diameter of each vertical line. The arithmetic mean of all these values is taken as the diameter of the corresponding part of the projectile. However, this estimated value represents diameter in image plane d_{image}. The required diameter in object plane d_{object} is given by:

$$d_{object} = d_{image} \times \frac{l}{resize\ factor} \qquad (8)$$

5. EXPERIMENTAL RESULTS

The silhouette of the projectile supplied by PXE, alongwith its different cylindrical parts is shown in Fig. 4. The diameter range at different parts of the projectile given by PXE is given in Table 1. For sub-pixel manipulation, existing interpolation algorithms like Nearest Neighbour, Bilinear, Bicubic, Lanczos2, Lanczos3, and authors two methods have been employed. The interpolation results for different portions of the projectile image are shown in Tables 2 to 6.

6. CONCLUSION

In this work the deformation of projectile is studied in flight through imaging. The projectile image is captured through a high speed acquisition device immediately it is fired near the muzzle. The image thus acquired suffers from motion blur. Considering the muzzle velocity and the shutter speed the blur length is computed and the point spread function is determined to approximate a de-blurred image. Various segments of the de-blurred projectile image are extracted to estimate the diameter. The proposed interpolation methods along with some of the existing standard interpolation methods are applied on the extracted segments and diameter is estimated. It is found that the proposed schemes have better accuracy than its counterparts.
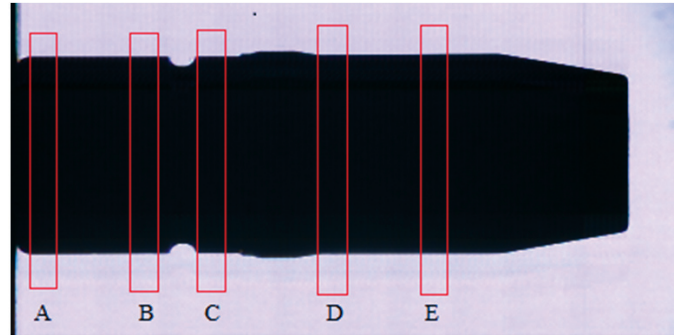

Figure 4. Silhouette of projectile image and its different portions.

Table 1. Diameter range of different portions of projectile, supplied by PXE

Cylindrical portion	Diameter range (in mm)
A	39.305 – 39.324
B	39.289 – 39.307
C	39.281 – 39.294
D	39.777 – 39.793
E	39.803 – 39.823

Table 2. Round 10: Portion 'A' (diameter in mm)

Resize factor	Nearest	Bilinear	Bicubic	Lanczos 2	Lanczos 3	Method 1	Method 2
1	39.458	39.458	39.458	39.458	39.458	39.458	39.458
2	39.458	39.148	39.286	39.192	39.198	39.317	39.317
3	39.458	39.251	39.251	39.251	39.251	39.277	39.277
4	39.458	39.303	39.303	39.303	39.303	39.315	39.314
5	39.458	39.328	39.332	39.331	39.331	39.319	39.314
6	39.458	39.254	39.299	39.274	39.273	39.312	39.314
7	39.458	39.281	39.281	39.281	39.281	39.314	39.314
8	39.458	39.301	39.303	39.301	39.301	39.313	39.314
9	39.458	39.297	39.317	39.302	39.303	39.313	39.314
10	39.458	39.273	39.300	39.286	39.285	39.314	39.314

Table 3. Round 10: Portion 'B' (diameter in mm)

Resize factor	Nearest	Bilinear	Bicubic	Lanczos 2	Lanczos 3	Method 1	Method 2
1	39.349	39.349	39.349	39.349	39.349	39.349	39.349
2	39.349	39.349	39.349	39.349	39.349	39.261	39.309
3	39.349	39.245	39.248	39.245	39.245	39.312	39.305
4	39.349	39.275	39.277	39.281	39.286	39.295	39.319
5	39.349	39.296	39.301	39.302	39.305	39.288	39.296
6	39.349	39.309	39.313	39.316	39.321	39.307	39.298
7	39.349	39.289	39.315	39.309	39.313	39.297	39.298
8	39.349	39.285	39.297	39.294	39.301	39.292	39.298
9	39.349	39.292	39.298	39.299	39.307	39.298	39.298
10	39.349	39.300	39.304	39.299	39.313	39.296	39.302

Table 4. Round 10: Portion 'C' (diameter in mm)

Resize factor	Nearest	Bilinear	Bicubic	Lanczos 2	Lanczos 3	Method 1	Method 2
1	39.349	39.349	39.349	39.349	39.349	39.349	39.349
2	39.349	39.349	39.349	39.349	39.349	39.260	39.232
3	39.349	39.349	39.349	39.349	39.349	39.269	39.257
4	39.349	39.222	39.290	39.255	39.251	39.274	39.269
5	39.349	39.230	39.246	39.238	39.245	39.315	39.270
6	39.349	39.245	39.254	39.250	39.250	39.296	39.283
7	39.349	39.260	39.262	39.261	39.262	39.296	39.283
8	39.349	39.271	39.271	39.271	39.271	39.309	39.298
9	39.349	39.277	39.280	39.280	39.280	39.309	39.290
10	39.349	39.269	125.287	39.283	39.281	39.308	39.302

Table 5. Round 10: Portion 'D' (diameter in mm)

Resize factor	Nearest	Bilinear	Bicubic	Lanczos 2	Lanczos 3	Method 1	Method 2
1	39.676	39.676	39.676	39.676	39.676	39.676	39.676
2	39.676	39.761	39.779	39.800	39.811	39.718	39.725
3	39.676	39.770	39.774	39.774	39.774	39.807	39.807
4	39.676	39.680	39.720	39.708	39.702	39.759	39.768
5	39.676	39.681	39.692	39.704	39.704	39.777	39.782
6	39.676	39.702	39.706	39.714	39.715	39.763	39.782
7	39.676	39.706	39.714	39.723	39.723	39.784	39.786
8	39.676	39.717	39.722	39.731	39.730	39.784	39.786
9	39.676	39.719	39.727	39.730	39.730	39.789	39.786
10	39.676	39.719	39.726	39.734	39.733	39.788	39.786

Table 6. Round 10: Portion 'E' (diameter in mm)

Resize factor	Nearest	Bilinear	Bicubic	Lanczos 2	Lanczos 3	Method 1	Method 2
1	39.678	39.678	39.678	39.678	39.678	39.678	39.678
2	39.678	39.785	39.797	39.818	39.818	39.782	39.822
3	39.678	39.768	39.769	39.768	39.773	39.808	39.808
4	39.678	39.759	39.762	39.771	39.773	39.806	39.810
5	39.678	39.770	39.778	39.784	39.795	39.802	39.808
6	39.678	39.765	39.782	39.796	39.809	39.801	39.815
7	39.678	39.771	39.793	39.811	39.820	39.801	39.813
8	39.678	39.781	39.804	39.811	39.813	39.805	39.818
9	39.678	39.777	39.801	39.807	39.808	39.806	39.818
10	39.678	39.782	39.799	39.810	39.810	39.808	39.819

REFERENCES

1. Gonzalez, Rafael C.; Woods, Richard Eugene & Steven, L. Eddins. Digital image processing using MATLAB. Pearson Education India, 2004.

2. Philippe, Thévenaz; Blu, Thierry & Unser, Michael. Image interpolation and resampling. 2000, 393-420. doi:10.1016/b978-012077790-7/50030-8

3. Shan, Y. & Goh, Wooi Boon. Sub-pixel location of edges with non-uniform blurring: a finite closed-form approach. *Image Vision comput.,* 2000, **18**(13), 1015-1023. doi:10.1016/S0262-8856(00)00040-8

4. Arandiga, F.; Donat, R. & Mulet, P. Adaptive interpolation of images. *Signal Proces.*, 2003, **83**(2), 459–464. doi:10.1016/S0165-1684(02)00445-0

5. Wong, Chi-Shing & Siu, Wan-Chi. Adaptive Directional Window Selection For Edge-Directed Interpolation. 19th International Conference on Computer Communications and Networks (ICCCN), IEEE, 2010. doi:10.1109/icccn.2010.5560064

6. Shezaf, Nira, Abramov-Segal, H.; Sutskover, I. & Bar-Sella, R. Adaptive low complexity algorithm for image zooming at fractional scaling ratio. The 21st IEEE Convention of the Electrical and Electronic Engineers in Israel. IEEE, 2000. doi:10.1109/eeei.2000.924383

7. Xiao, Jianping; Zou, Xuecheng; Liu, Zhenglin & Guo, Xu. Adaptive interpolation algorithm for real-time image resizing. *In* First International Conference on Innovative Computing, Information and Control, 2006. ICICIC'06. IEEE, 2, 2006. doi:10.1109/icicic.2006.226

8. Zhang, Xiangjun, and Xiaolin Wu. Image interpolation by adaptive 2-D autoregressive modeling and soft-decision estimation. *IEEE Trans. Image Proces.*, 2008, 17(6), 887-896. doi:10.1109/TIP.2008.924279

9. Luong, Hiêp; Ledda, Alessandro & Philips, Wilfried. An image interpolation scheme for repetitive structures. *In* Image Analysis and Recognition. Springer Berlin Heidelberg, 2006, 104-115. doi:10.1007/11867586_10

10. Muhammad, Sajjad; Ejaz, Naveed & Baik, Sung Wook. Multi-kernel based adaptive interpolation for image super-resolution. *Multimedia Tools Appli.*, 2012, **72**(3), 1-23. doi:10.1007/s11042-012-1325-4

11. Richardson, William Hadley. Bayesian-based iterative method of image restoration. *JOSA* 1972, **62**(1), 55-59. doi:10.1364/JOSA.62.000055

12. Sa, Pankaj Kumar, Dash, Ratnakar; Majhi, Banshidhar & Panda, Ganapati. Improved iterative blind image deconvolution. *In* Advances in Numerical Methods. Springer US, 2009. 271-278. doi: 10.1007/978-0-387-76483-2_23

CONTRIBUTORS

Mr Suman Kumar Choudhury obtained his BTech (CSE) from BPUT, Rourkela in 2010 and MTech (CSE) from NIT, Rourkela, in 2013.He is currently pursuing his doctoral research at NIT, Rourkela, in the area of video surveillance. His areas of interest include image processing, computer vision and pattern recognition.

Dr Pankaj Kumar Sa received his MTech (CSE) and PhD (Image Processing) from NIT, Rourkela. He is working as Assistant Professor in the Department of Computer Science and Engineering, NIT Rourkela. He has 08 years of teaching and research experience. His research interest also includes computer vision and computer graphics.

Mr Tapan Kumar Biswal is currently working as a scientist at the Proof & Experimental Establishment, Chandipur. He has 30 years of experience in the domain of high speed imaging and photonics. His research interests include high speed imaging and sensors.

Mr Banshishar Majhi is working as a professor in the Department of Computer Science and Engineering, NIT, Rourkela. He has 24 years of teaching and research experience. His research interests include image processing, computer vision, and iris biometrics.